IEEE Access
Multidisciplinary ⋮ Rapid Review ⋮ Open Access Journal

Received March 27, 2021, accepted April 19, 2021, date of publication April 26, 2021, date of current version April 30, 2021.

Digital Object Identifier 10.1109/ACCESS.2021.3075433

A Computational Method to Estimate the Effect of Gold Nanoparticles on X-Ray Induced Dose Enhancement and Double-Strand Break Yields

YA-YUN HSIAO[1,2], FENG-CHUN TAI[3], CHUN-CHIEH CHAN[3], AND CHING-CHIH TSAI[3], (Fellow, IEEE)

[1]Department of Medical Imaging and Radiological Sciences, Chung Shan Medical University, Taichung 40201, Taiwan
[2]Department of Medical Imaging, Chung Shan Medical University Hospital, Taichung 40201, Taiwan
[3]Department of Electrical Engineering, National Chung Hsing University, Taichung 40227, Taiwan

Corresponding authors: Ching-Chih Tsai (cctsai@nchu.edu.tw) and Chun-Chieh Chan (andyccc0915@gmail.com)

This work was supported in part by Chung Shan Medical University, in part by the Chung Shan Medical University Hospital, and in part by the Ministry of Science and Technology, Taiwan, under Contract MOST 109-2218-E-005-013.

ABSTRACT We report the effects of gold nanoparticles (GNP) on the enhancement of the dose effect and double-strand break (DSB) induction for X-ray monoenergies (10 keV–2 MeV). The overall relative biological effectiveness (RBE) was defined as the product of dose and DSB enhancement. The cellular doses and energy spectra were computed using the PENELOPE (PENetration and Energy LOss of Positrons and Electrons) code. The DNA damage yields were estimated using the MCDS (Monte Carlo damage simulation) code. Considering the production of Auger electrons induced by 7mg/ml GNP, we found that dose enhancement at the 30 keV was ∼4.0 for cells with radius 4 μm. The DSB induction increased as GNP concentrations increased and was dependent on X-ray energy. These findings demonstrated that the maximum RBE was attained at 30–40 keV and therefore this energy range would be more efficient in cancer cell killing.

INDEX TERMS Relative biological effectiveness, gold nanoparticle.

I. INTRODUCTION

High-Z materials have been studied for the enhancement of radiation dose for over 60 years [1]. This enhancement is possible because of higher cross-sections in the photoelectrical effects of high-Z materials. An example of a high-Z material is iodine (Z = 53), which has been shown to exhibit a radiosensitisation effect when used as a contrast agent in imaging [2], [3]. The iodine agents imposed some limitations such as occasional renal toxicity, rapid renal clearance, and short imaging times. Meanwhile, gold (Z = 70) is another high-Z material, and gold nanoparticles (GNP) have recently been widely used in diverse applications such as imaging [3], biological studies [4], and chemical synthesis because of their biocompatibility and longer imaging times, and unique physicochemical properties such as surface plasmon resonance [5]–[7]. GNP radiosensitization was demonstrated both *in vitro* and *in vivo*. *In vitro*, GNP radiosensitization has been observed in cells [8], plasmid DNA [9], and Monte Carlo simulations [10]–[12]. *In vivo*, Hainfeld *et al.* [13] showed that GNP could increase long-term survival of mice bearing EMT-6 mammary carcinomas after 250 keV photon irradiation and injection of 1.9 nm GNP. Studies have also shown that dose enhancement of GNP was associated with increased effectiveness in cancer killing and reduced tumor growth [5], [14].

The dose enhancement of GNP in the cells under X-ray irradiation was shown to be dependent on several parameters, such as GNP size, cell radius, and GNP concentration and distribution in cells [5], [10], [15]. Different phantom geometries were used and the range is from micrometer [10] to centimeter [16]. Furthermore, the resonant structures of gold corresponding to K_α and K_β are within 67–80 keV [17], when cells containing GNPs are irradiated with 67–80 keV X-rays, photons would produce a resonance that induces a large cascade of photoelectrons, Auger electrons, and their secondary particles through energy-loss processes. Detailed resonant structures corresponding to K_α at 68 keV [17] coupled with a higher peak in electron counts was observed in comparison with that at K_β (82 keV) [18]. Ionizing radiations such as

The associate editor coordinating the review of this manuscript and approving it for publication was Ravibabu Mulaveesala.

X-rays and electrons can induce DNA damage through direct and indirect mechanisms [19]. That is, X-rays may directly ionize or excite the atoms of DNA, or alternatively, X-rays may interact with water or cell medium to produce secondary electrons and free radicals to induce damage to DNA [20]. These low-energy electrons produced at K_α and K_β could be more effective in DNA damage induction [21], [22] and therefore can be used to increase cancer cell killing, consequently increasing the therapeutic index.

For GNP radiosensitization application, it is important to quantify the relative biological effectiveness (RBE) of radiation doses and the associated biological markers such as DNA double-strand break (DSB) for improved correlation between GNP dose enhancement and cancer cell killing. To the best of our knowledge, this article is the first to report on the enhancement of the dose effect and DSB induction in the imaging range around the K-edge (∼80.7 keV). Our results show that dose enhancement decreased as photon energy (>40 keV) increased; however, there was a small peak around the K-edge with corresponding enhancements of 1.2 (at 68 keV) and 1.4 (at 82 keV), respectively. The DSB induction (per Gy per Gbp) showed little difference (<5%) for all energies applied in this report.

II. MATERIAL AND METHOD

A. CELL MODEL AND GNP DENSITIES

The cellular target is a representative mammalian cell modeled by a water sphere with radius 4 μm. The size of nuclear radius (∼4 μm) is the typical size of V79 Chinese hamster cells used in many experiments [23], [24]. Several *in vivo* studies used mice in GNP experiments [13], [25], [26], therefore we also chose hamster cells to mimic the experimental conditions.

The density of the gold-loaded cellular target was increased from 1.0 g cm^{-3} to the value reflecting the added weight of gold (e.g., 1.007 g cm^{-3} for cells loaded with 7 mg Au g^{-1}). GNP concentrations ranging from 0.01 to 70 mg/ml were used for simulations, as previously done in vitro and in vivo studies [13], [25], [27] and simulations [10], [18]. We followed the approach used by [16] and did not explicitly consider the dependency on particle size and shape. That is, this approach only considers the water (or tissue) phantom with the presence of GNPs at different concentration levels to estimate the macroscopic dose enhancement. The dose enhancement shown in this study is due to the difference in mass absorption coefficients between gold and water. In this case, the mono-energetic electrons (see below) clearly demonstrate the effect.

B. PENELOPE

The penmain program in PENELOPE code (2011 version) [28] was used to calculate the deposited amount of photon energies (10, 15, 40, 68, 69, 82, and 250 keV and 2 MeV) in cells. The photon energies used in this study are all mono-energetic. The actual electron emission point and its related path were both determined using random numbers. All primary and secondary electrons were followed down to 50 eV. PENELOPE has been proven to provide accurate calculations at subcellular doses [29]. This code applies a mixed simulation algorithm for electron and positron interactions, that is, event-by-event simulation for hard collisions and multiple scattering theory for soft collisions. This mixed algorithm [30] permits a fast simulation of electron and positron transport in matter. In addition, the modified version of PENELOPE 2011 adopts a more realistic continuous energy-loss distribution to replace the previous discrete optical oscillator-strength model. This modification improves both the reliability and generality of the code [28]. The statistical uncertainties in dose calculation and the fluence derived by PENELOPE code are below 2% and 10%, respectively.

C. MONTE CARLO DAMAGE SIMULATION

The Monte Carlo Damage Simulation (MCDS) method was used to provide estimates of the yield of clustered damage in cells after irradiation with photons, monoenergetic electrons, protons, and heavy ions up to ^{56}Fe ions [31]–[33]. In a constant target (cell nucleus) exposed to a dose of 1 Gy, the MCDS algorithm can simulate the yields for different types of DNA damage. This algorithm reported DNA damage data and captured the major trends of DNA damage spectra from detailed track structure simulations. Because the damage yields simulated by the MCDS code implicitly account for DNA damage clusters caused by primary charged particles and secondary electrons in a typical mammalian cell, damage yields can be determined by weighting the yields by the fluence of primary charged particles. The uncertainty in DSB yields derived by MCDS is below 0.2%.

D. CALCULATION OF DSB DAMAGE

The amount of DSB damage Y was calculated by using the formula for dose-weighted DSB [34]:

$$\mathrm{Y} = \frac{\int_0^\infty dEY\,(E)\,\Phi\,(E)\,\mathrm{LET}_\infty\,(E)}{\int_0^\infty dE\,\Phi\,(E)\,\mathrm{LET}_\infty\,(E)} \tag{1}$$

where $Y(E)$ is the yield of total DSB clusters per Gy per gigabase pairs (per Gy per Gbp) with electrons of energy E, Φ is the total fluence of secondary electrons produced in the cell medium through interactions with X-rays, and $\Phi(E)$ is the energy fluence of secondary electrons of energy E. For electrons with energies higher than 1 keV, unrestricted linear energy transfer (*LET*) (stopping powers) from the National Institute of Standards and Technology was used [35].

E. RELATIVE BIOLOGICAL EFFECTIVENESS (RBE)

RBE is usually defined as the ratio of the dose of a low LET reference radiation to the dose of another radiation needed to achieve the same biological effect. Because the induction of DNA damage is proportional to the absorbed dose D, up to at least a few hundred Gy of low and high LET radiation [36]–[38], RBE can also be defined as the ratio of

TABLE 1. Dose enhancement and DSB induction for cells with 4 μm radius irradiated with 82 keV photons relative to various GNP concentrations.

GNP Concentration (mg/ml)	DSB (per Gy per Gbp)	Dose enhancement	DSB Induction Enhancement	RBE
0	9.16	1.0	1.00	1.0
0.01	9.18	1.0	1.00	1.0
0.1	9.18	1.0	1.00	1.0
7	9.26	1.5	1.01	1.5
14	9.35	1.9	1.02	1.9
35	9.48	3.1	1.03	3.3
56	9.49	4.4	1.04	4.5
70	9.51	5.1	1.04	5.3

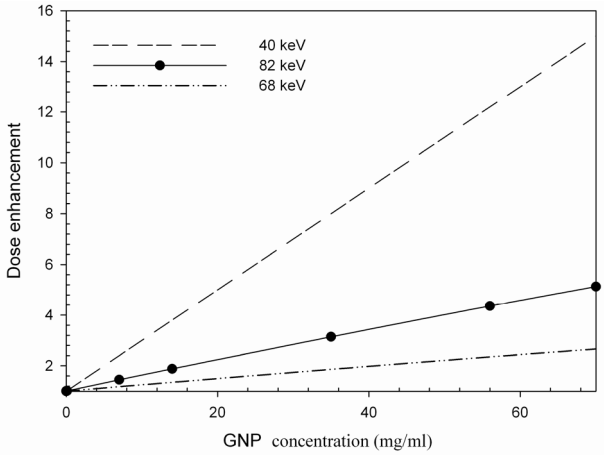

FIGURE 1. Dose enhancement versus GNP concentrations for cells with 4 μm radius irradiated with 40, 82 and 68 keV X-rays, respectively.

the damaged yields of cells irradiated with different radiation sources, as shown below:

$$RBE = \frac{D_R}{D_e} = \frac{\Sigma_e}{\Sigma_R} \tag{2}$$

The subscripts, e and R, respectively denote electrons with energy E and reference radiation. The DSB yield for cells irradiated by 250 keV X-rays is the reference for all reported RBE values. Here, because GNP would increase both dose and DSB induction, RBE was defined as the ratio of the product of dose and DSB yields of cells containing GNP to the product of dose and DSB yields of cells containing water only.

III. RESULTS

Fig. 1 first shows that dose enhancement was linearly proportional to GNP concentrations (0–70 mg/ml). The slope of the linear relationship was dependent on energy. The results of 40, 82 and 68 keV X-rays were listed. The slope of 40 keV is the highest and followed by 82 and 68 keV. Since the K-shell of gold lied at 80.7 keV, the slope was higher for 82 keV X-rays than that for 68 keV X-rays. Next, the relationship between dose enhancement and photon energy for cells containing 7 and 70 mg/ml GNP, respectively, is presented in Fig. 2. Dose enhancement showed an increase

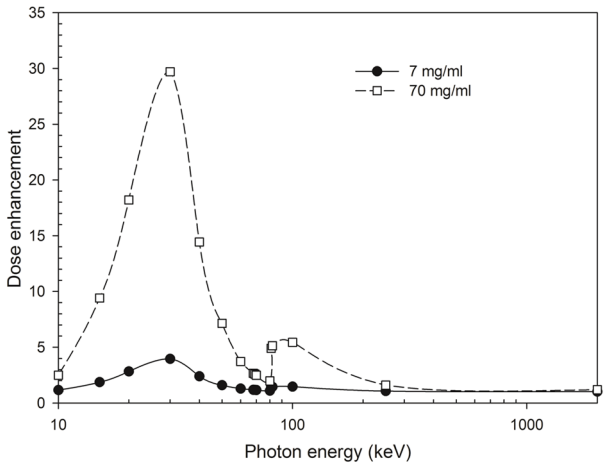

FIGURE 2. Dose enhancement versus photon energy for cells with 4 μm radius containing 7 mg/ml and 70 mg/ml GNP.

starting at 10 keV X-rays until it reached a maximum increase of 4 for 7 mg/ml GNP and 29.7 for 70 mg/ml GNP at 30 keV X-ray and was then followed by sharp decrease until the K-edge of gold (80.7 keV). After passing the K-edge, dose enhancement significantly increased from 1.1 to 1.4 for 7 mg/ml GNP and from 2.0 to 4.9 for 70 mg/ml GNP. However, dose enhancement decreased to 1.0 for photon energies higher than 250 keV for both GNP concentrations. Later we combined the dose enhancement, DSB induction (per Gy per Gbp), and RBE for cells with 4 μm radius irradiated with 82 keV photons for various concentrations of GNP (0–70 mg/ml) in Table 1. As mentioned previously, dose enhancement was linearly proportional to GNP concentrations (Fig. 1). At 7 mg/ml GNP, a concentration used in animal treatment by Hainfeld *et al.* [13], [25], RBE was 1.5. For very low GNP concentrations (<1 mg/ml), RBE did not exceed 1.0 and therefore may not have any significant effects. Furthermore, the dose-weighted DSB induction displayed only a slight increase as GNP concentration increased. DSB yields were roughly constant (~9.16–9.51 per cell per Gy) and only showed a 4% increase relative to water even at the highest GNP concentration (70 mg/ml). This could be because the energy of most secondary electrons for 82 keV X-rays is higher than 5 keV and has a roughly constant DSB induction [32]. Nevertheless, for higher GNP concentrations, average secondary electron energies are expected to be lower since more photoelectrons are produced in the K shell ($82-80.7 = 1.3$ keV) with a small increase in the L shell ($82-10.7 = 71.3$ keV). At 7 mg/ml GNP, ~23% of electrons were less than 5 keV versus ~20% of electrons for water only, whereas at 70 mg/ml GNP, ~28% of electrons were less than 5 keV and therefore the DSB induction (per Gy per Gbp) was higher for higher GNP concentrations.

To find the maximum RBE, we then calculated the dose enhancement and DSB induction (per Gy per Gbp) for cells containing 7 mg/ml GNP after irradiation with various photon energies (10 keV–2 MeV) shown in Table 2. As shown

TABLE 2. Dose enhancement and DSB induction for cells with 4 μm radius containing 7 mg/ml GNP or water irradiated with various photon energies.

Energy (keV)	DSB of GNP (per Gy per Gbp)	DSB of water (per Gy per Gbp)	Dose enhancement to water	DSB enhancement to water	RBE
10	9.75	9.72	1.2	1.00	1.2
15	9.43	9.16	1.9	1.03	1.9
20	9.22	8.81	2.8	1.05	3.0
30	9.02	8.73	4.0	1.03	4.1
40	8.99	9.11	2.4	0.99	2.4
50	9.22	9.58	1.6	0.96	1.5
60	9.35	9.62	1.3	0.97	1.3
68	9.29	9.48	1.2	0.98	1.2
69	9.34	9.49	1.2	0.98	1.2
70	9.29	9.44	1.2	0.98	1.1
80	9.17	9.23	1.1	0.99	1.1
81	9.33	9.25	1.4	1.01	1.4
82	9.26	9.16	1.5	1.01	1.5
100	8.92	8.93	1.5	1.00	1.5
250	8.37	8.38	1.1	1.00	1.1
2000	8.14	8.15	1.0	1.00	1.0

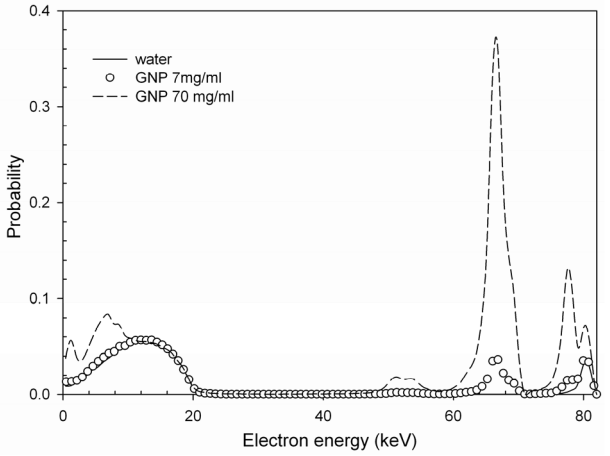

FIGURE 3. Electron spectra for cells with 4 μm radius irradiated by 82 keV X-rays containing 7 mg/ml, 70 mg/ml GNP and water only. The probability is normalized by the total probability of electron spectra of cells containing water only.

in Fig. 2, the highest dose enhancement occurred at 30 keV, followed by a decrease to 1.2 at ∼68 keV, and an increase to 1.5 at 82 keV because of the K-edge effect. However, for higher photon energies (250 keV and 2 MeV), RBE was approximately 1. At 82 keV, the major difference between the electron spectra of cells containing GNP and those containing only water was the counts of secondary electrons in the ranges 0–10 keV and 50–82 keV, which was 5% and 18% more, respectively, for cells containing 7 mg/ml GNP. These higher energy electrons (50–82 keV) are the photoelectrons produced at the L shell. As GNP concentration increased, more electrons appeared in the 0–10 keV range and small peaks were observed in the 50–82 keV range for spectra containing GNP only (Fig. 3).

Moreover, from Table 2, the enhancement value of DSB induction relative to water was ∼1.0 and slightly larger at low energies, indicating that the addition of GNP had no significant effect on the DSB induction. The trend of RBE was similar to that of dose enhancement. DSB induction was higher at very low photon energies (<15 keV); for example, the DSB yield at 10 keV was 9.75 per Gy per Gbp and about 8% higher than the DSB induction at 30 keV. However, the DSB induction (per cell per Gy) at 30 keV was lower than that of higher photon energies at 68 keV and 82 keV. That is due to the production of Auger electrons at 68 and 82 keV X-ray irradiation and the contribution of these lower energy electrons to the yields of DSB induction. For megavoltage photon energies, the energy of most secondary electrons was more than 5 keV and DSB induction decreased to 8.1 per Gy per Gbp, suggesting that GNP may have weaker effects for higher energy electrons.

IV. DISCUSSION

We investigated the enhancement of the dose effect and DSB induction (per Gy per Gbp) for cells of 4 μm in radius irradiated with a range of photon energies (10 keV–2 MeV). Compared with the study by Cai *et al.* [10] whose radius of cell nucleus is 6.3 μm, the dose enhancement using our approach (with the same radius) is ∼1.4 and is in good agreement with Cai's calculated values 1.3 (Table 1 in Cai's study) for the concentration of 7 mg/ml in cells irradiated with 100 keV X-rays. For DSB induction, the RBE of cells mixed with GNP irradiated by 80 keV X-rays is reported to be in the range of 1.05–1.17 [39] while our result is 1.1 (Table 2).

Further, we found that dose enhancement was dependent on photon energy (Fig. 1) and linearly proportional to GNP concentrations (Table 1), which is in agreement to what was previously reported by Montenegro *et al.* [18] and Cai *et al.* [10]. In Fig. 1, the slopes of the 3 curves (68, 82, 40 keV) are linearly proportional to the ratio of the mass absorption coefficients of water containing GNP to those of water only. This result suggest that ratio is higher for 40 keV X-rays than those for 68 and 82 keV X-rays. However, the maximum dose enhancement has been reported to be around 40–50 keV [40] due to the fact that the maximum relative mass absorption coefficient of gold to water is at around 40–50 keV. One explanation for this difference is that the electrons with energies less than 30 keV deposit most of their energies in smaller cells while higher energy electrons such as 40 keV may deposit part of their energies outside the cells, leading to a higher energy requirement for dose enhancement for larger cells. This explanation can be supported by the information: the ranges of 30 and 40 keV electrons are respectively 16.8 μm and 27.6 μm [41]. Besides the dose enhancement, the biological effects for cells irradiated with X-rays needs to consider the effects of HO· radicals [19] and the overall effects would swift the range of maximum to 30–50 keV [15].

Table 2 shows that the yields of DSB induction are getting smaller when the GNP is present as photon energy increases from 40 keV to 60 keV. That is because the yields of DSB

induction is correlated with the number of low-energy electrons, especially for those electrons with energy less than 5 keV [24]. The higher the photon energy, the less the DSB yields. However, the yields are increased as photon energy increases from 60 keV to 82 keV. That is due to the fact the resonant structures of gold corresponding to K_α and K_β are about 68 and 80 keV, respectively [17]. When the water medium (mixed with GNPs) was irradiated by 68 or 80 keV, the yields of auger electrons (energy less than 5 keV) would increase dramatically and hence the yields of DSB induction would also be increased.

As shown in Fig. 3, because a larger number of Auger electrons are produced around the K-edge, as suggested by Montenegro *et al.* [18], local maximum RBE may occur around the K-edge. However, in our study, the total number of electrons with energies less than 5 keV for 30 keV was twice that for 82 keV and hence can be more efficient in cancer cell killing. These results suggest that the optimal range for photon energy exposure to tumor cells is 30–40 keV and the use of Auger electrons emitting by K-edge effects would require a small cavity whose size is in the range of 1 nm to 1 μm [42] and subcellular delivery [43] of high concentrations of GNP such as 70 mg/ml to induce large Auger electrons production as shown in Fig. 3. This requirement also sets a limitation to our method due to the difficulty in measuring the doses at a micrometer resolution. For higher energies (100 keV–2MeV), the level of RBE and DSB induction was $\sim$1, indicating that the overall effect is not obvious.

Besides photon energy, other factors also affect the dose enhancement and RBE. Because the cell model is composed by water, the simulation results may exhibit some difference in dose estimation from the results using tissues. It has been reported that the difference between in the dose in water and the dose in tissue (adipose, muscle, and skin, etc.) is in the range 3–70% [44]. It is certainly that the estimated dose in this study may be underestimated for some tissue types. For example, the ratio of dose in adipose to the dose in water is $\sim$1.7. That is because some tissue types such as adipose have higher mass absorption coefficients.

In the previous studies, the concentration $\sim$0.01 mg/ml was used in cell dishes [27] and the concentrations 7–74 mg/ml were used in tumors in the thighs of mice with no apparent short- or long-term toxicity [13], [25], [26]. For example, it has been showed that the concentration 7 mg/ml increased tumor doubling time 58% and long-term survivors (mice) from 0–38% [13], [25] and the concentration 74 mg/ml also prolonged cell survival with statistical significance ($P < 0.05$) [26]. *In vitro* studies show the dose enhancement is in the range of 1.0005$\sim$1.05 for the concentration 1 nM$\sim$1 mM, depending on the radiation sources [45]. Our choice is in accordance with the *in vivo* studies, i.e., 7$\sim$70 mg/ml. The concentrations used in the Monte Carlo simulations were up to 200 mg/ml [10], [18]. The overall reported concentrations of the GNP were in the range of 0.01 mg/ml (1 nM) to 17000 mg/ml (1 mM) [45]. Moreover, the toxicity tests showed that there is no evidence of toxicity in 30 days for mice initially injected with a concentration 10 mg/ml of GNPs [46]. A recent *in vitro* study done by Carnovale *et al.* (2019) reported that the cell viability is not affected when the concentration of GNP is within 10 μM ($\sim$170 mg/ml) [47].

For very low concentrations of GNP (0.01–0.1 mg/ml), a small increase ($<$1%) was observed in the enhancement of the dose effect and DSB induction (see Table 1). But a previous study by Chithrani *et al.* [26] mentioned the application of very low GNP concentrations, in which it was shown that the enhancement of DSB induction in Hela cells containing 10^{-3}% of 50 nm GNP ($\sim$0.0088 mg/ml) was 1.66 and 1.17 after irradiation with 105 kVp and 6 MVp photons, respectively. Another study also showed that the survival rate of cancer cells dropped from 1 to 0.38 after 2 h exposure to low concentrations (5–20 nM, 0.1–0.4 mg/ml) of 15 nm GNP for prostate carcinoma cells irradiated with ^{137}Cs (662 keV) [48]. Their concentrations are as low as our concentration 0.01 mg/ml yet the enhancement of DSB induction are considerable higher than our simulated results ($\sim$1) for the energies above 100 keV. These contradictions may indicate the RBE for biological endpoints may largely rely on the biological characteristics other than physical quantity.

In summary, we reported the enhancement of the dose effect and DSB induction for cells containing 7 mg/ml GNP and irradiated with a photon energy range of 10 keV–2 MeV. The maximum dose enhancement and DSB induction occurred at 30 keV and 10 keV, respectively. The DSB induction around the K-edge (82 keV) was $\sim$3% higher than that of 30 keV, indicating that the production of Auger electrons can slightly increase the yields of DSB induction around the K-edge. The maximum RBE was attained in the energy range of 30–40 keV, whereas for megavoltage energies, both RBE and DSB induction levels were $\sim$1.

ACKNOWLEDGMENT

The authors thank Dr. Shu-Ju Tu of Chang Gung University, Taiwan, for insightful discussions.

REFERENCES

[1] F. W. Spiers, "The influence of energy absorption and electron range on dosage in irradiated bone," *Brit. J. Radiol.*, vol. 22, pp. 521–533, Sep. 1949.

[2] L. Caschera, A. Lazzara, L. Piergallini, D. Ricci, B. Tuscano, and A. Vanzulli, "Contrast agents in diagnostic imaging: Present and future," *Pharmacol. Res.*, vol. 110, pp. 65–75, Aug. 2016.

[3] J. F. Hainfeld, D. N. Slatkin, T. M. Focella, and H. M. Smilowitz, "Gold nanoparticles: A new X-ray contrast agent," *Brit. J. Radiol.*, vol. 79, no. 939, pp. 248–253, Mar. 2006.

[4] M. H. Kim, "Nanoparticle-based therapies for wound biofilm infection: Opportunities and challenges," *IEEE Trans. Nanobiosci.*, vol. 15, no. 4, pp. 294–304, Apr. 2016.

[5] S. Jain, D. G. Hirst, and J. M. O'Sullivan, "Gold nanoparticles as novel agents for cancer therapy," *Brit. J. Radiol.*, vol. 85, pp. 13–101, Feb. 2012.

[6] E. E. Connor, J. Mwamuka, A. Gole, C. J. Murphy, and M. D. Wyatt, "Gold nanoparticles are taken up by human cells but do not cause acute cytotoxicity," *Small*, vol. 1, pp. 325–327, Mar. 2005.

[7] N. Agrawal, B. Zhang, C. Saha, C. Kumar, B. K. Kaushik, and S. Kumar, "Development of dopamine sensor using silver nanoparticles and PEG-functionalized tapered optical fiber structure," *IEEE Trans. Biomed. Eng.*, vol. 67, no. 6, pp. 1542–1547, Jun. 2020.

[8] D. F. Regulla, L. B. Hieber, and M. Seidenbusch, "Physical and biological interface dose effects in tissue due to X-ray-induced release of secondary radiation from metallic gold surfaces," *Radiat. Res.*, vol. 150, pp. 92–100, Jul. 1998.
[9] Y. Zheng and L. Sanche, "Gold nanoparticles enhance DNA damage induced by anti-cancer drugs and radiation," *Radiat. Res.*, vol. 172, pp. 114–119, Jul. 2009.
[10] Z. Cai, J. P. Pignol, N. Chattopadhyay, Y. L. Kwon, E. Lechtman, and R. M. Reilly, "Investigation of the effects of cell model and subcellular location of gold nanoparticles on nuclear dose enhancement factors using Monte Carlo simulation," *Med. Phys.*, vol. 40, p. 114101, Nov. 2013.
[11] E. Lechtman, N. Chattopadhyay, Z. Cai, S. Mashouf, R. Reilly, and J. P. Pignol, "Implications on clinical scenario of gold nanoparticle radiosensitization in regards to photon energy, nanoparticle size, concentration and location," *Phys. Med. Biol.*, vol. 56, pp. 4631–4647, Aug. 2011.
[12] P. Retif, T. Bastogne, and M. Barberi-Heyob, "Robustness analysis of a geant4-GATE simulator for nanoradiosensitizers characterization," *IEEE Trans. Nanobiosci.*, vol. 15, pp. 209–217, Apr. 2016.
[13] J. F. Hainfeld, D. N. Slatkin, and H. M. Smilowitz, "The use of gold nanoparticles to enhance radiotherapy in mice," *Phys. Med. Biol.*, vol. 49, no. 18, pp. N309–N315, Sep. 2004.
[14] K. Haume, "Gold nanoparticles for cancer radiotherapy: A review," *Cancer Nanotechnol*, vol. 7, p. 8, Nov. 2016.
[15] E. Brun, L. Sanche, and C. Sicard-Roselli, "Parameters governing gold nanoparticle X-ray radiosensitization of DNA in solution," *Colloids Surf. B Biointerfaces*, vol. 72, pp. 34–128, Aug. 2009.
[16] S. H. Cho, B. L. Jones, and S. Krishnan, "The dosimetric feasibility of gold nanoparticle-aided radiation therapy (GNRT) via brachytherapy using low-energy gamma-/X-ray sources," *Phys. Med. Biol.*, vol. 54, pp. 4889–4905, Aug. 2009.
[17] A. K. Pradhan, "Resonant X-ray enhancement of the Auger effect in high-Z atoms, molecules, and nanoparticles: Potential biomedical applications," *J. Phys. Chem. A*, vol. 113, pp. 12356–12363, Nov. 2009.
[18] M. Montenegro, S. N. Nahar, A. K. Pradhan, K. Huang, and Y. Yu, "Monte Carlo simulations and atomic calculations for Auger processes in biomedical nanotheranostics," *J. Phys. Chem. A*, vol. 113, pp. 12364–12369, Nov. 2009.
[19] E. J. Hall and A. J. Giaccia, *Radiobiology for the Radiologist*, 7th ed. Philadelphia, PA, USA: Wolters Kluwer Health/Lippincott Williams & Wilkins, 2012.
[20] A. K. Holley, L. Miao, D. K. St Clair, and W. H. St Clair, "Redox-modulated phenomena and radiation therapy: The central role of superoxide dismutases," *Antioxid Redox Signal*, vol. 20, pp. 1567–1589, Apr. 2014.
[21] D. T. Goodhead, "Initial events in the cellular effects of ionizing radiations: Clustered damage in DNA," *Int. J. Radiat. Biol.*, vol. 65, no. 1, pp. 7–17, Jan. 1994.
[22] J. F. Ward, "The complexity of DNA damage: Relevance to biological consequences," *Int. J. Radiat. Biol.*, vol. 66, no. 5, pp. 427–432, Jan. 1994.
[23] A. I. Kassis, "The amazing world of auger electrons," *Int. J. Radiat. Biol.*, vol. 80, nos. 11–12, pp. 789–803, Jan. 2004.
[24] Y.-Y. Hsiao, T.-H. Hung, S.-J. Tu, and C.-J. Tung, "Fast Monte Carlo simulation of DNA damage induction by auger-electron emission," *Int. J. Radiat. Biol.*, vol. 90, no. 5, pp. 392–400, May 2014.
[25] J. F. Hainfeld, F. A. Dilmanian, Z. Zhong, D. N. Slatkin, J. A. Kalef-Ezra, and H. M. Smilowitz, "Gold nanoparticles enhance the radiation therapy of a murine squamous cell carcinoma," *Phys. Med. Biol.*, vol. 55, pp. 3045–3059, Jun. 2010.
[26] M. Y. Chang, A. L. Shiau, Y. H. Chen, C. J. Chang, H. H. Chen, and C. L. Wu, "Increased apoptotic potential and dose-enhancing effect of gold nanoparticles in combination with single-dose clinical electron beams on tumor-bearing mice," *Cancer Sci*, vol. 99, pp. 1479–1484, Jul. 2008.
[27] D. B. Chithrani, "Gold nanoparticles as radiation sensitizers in cancer therapy," *Radiat. Res.*, vol. 173, pp. 719–728, Jun. 2010.
[28] F. Salvat, J. M. Fernández-Varea, and J. Sempau, *PENELOPE 2011: A Code System for Monte Carlo Simulation of Electron and Photon Transport*. Issy-les-Moulineaux, France: OECD Nuclear Energy Agency, 2011.
[29] R. D. Stewart, W. E. Wilson, J. C. McDonald, and D. J. Strom, "Microdosimetric properties of ionizing electrons in water: A test of the PENELOPE code system," *Phys. Med. Biol.*, vol. 47, no. 1, pp. 79–88, Jan. 2002.
[30] J. Baró, J. Sempau, J. M. Fernández-Varea, and F. Salvat, "PENELOPE: An algorithm for Monte Carlo simulation of the penetration and energy loss of electrons and positrons in matter," *Nucl. Instrum. Methods Phys. Res. B, Beam Interact. Mater. At.*, vol. 100, no. 1, pp. 31–46, May 1995.
[31] V. A. Semenenko and R. D. Stewart, "A fast Monte Carlo algorithm to simulate the spectrum of DNA damages formed by ionizing radiation," *Radiat. Res.*, vol. 161, no. 4, pp. 451–457, Apr. 2004.
[32] V. A. Semenenko and R. D. Stewart, "Fast Monte Carlo simulation of DNA damage formed by electrons and light ions," *Phys. Med. Biol.*, vol. 51, pp. 1693–1706, Apr. 2006.
[33] R. D. Stewart, V. K. Yu, A. G. Georgakilas, C. Koumenis, J. H. Park, and D. J. Carlson, "Effects of radiation quality and oxygen on clustered DNA lesions and cell death," *Radiat. Res.*, vol. 176, pp. 587–602, Nov. 2011.
[34] Y. Hsiao and R. D. Stewart, "Monte Carlo simulation of DNA damage induction by x-rays and selected radioisotopes," *Phys. Med. Biol.*, vol. 53, pp. 233–244, Jan. 2008.
[35] M. J. J. S. Berger Coursey, M. A. Zucker, and J. Chang. (Jan. 1999). *PSTAR, and ASTAR: Computer Programs for Calculating Stopping-Power and Range Tables for Electrons, Protons, and Helium Ions*. [Online]. Available: http://physics.nist.gov/Star
[36] D. Frankenberg, "Induction of DNA double-strand breaks by 1H and 4He ions in primary human skin fibroblasts in the LET range of 8 to 124 keV/μm," *Radiat. Res.*, vol. 151, pp. 540–549, May 1999.
[37] B. M. Sutherland, P. V. Bennett, J. C. Sutherland, and J. Laval, "Clustered DNA damages induced by X-rays in human cells," *Radiat. Res.*, vol. 157, no. 6, pp. 611–616, Jun. 2002.
[38] K. Rothkamm and M. Lobrich, "Evidence for a lack of DNA double-strand break repair in human cells exposed to very low X-ray doses," *Proc. Natl. Acad. Sci. USA*, vol. 100, pp. 5057–5062, Apr. 2003.
[39] R. Liu, T. Zhao, X. Zhao, and F. J. Reynoso, "Modeling gold nanoparticle radiosensitization using a clustering algorithm to quantitate DNA double–strand breaks with mixed-physics Monte Carlo simulation," *Med. Phys.*, vol. 46, no. 11, pp. 5314–5325, Nov. 2019.
[40] A. Mesbahi, "A review on gold nanoparticles radiosensitization effect in radiation therapy of cancer," *Rep. Pract. Oncol. Radiother*, vol. 15, pp. 176–180, Oct. 2010.
[41] M. Siragusa, G. Baiocco, P. M. Fredericia, W. Friedland, T. Groesser, A. Ottolenghi, and M. Jensen, "The COOLER code: A novel analytical approach to calculate subcellular energy deposition by internal electron emitters," *Radiat. Res.*, vol. 188, no. 2, pp. 204–220, Aug. 2017.
[42] F. Paquet, P. Barbey, M. Bardiès, A. Biau, E. Blanchardon, A. Chetioui, L. Lebaron-Jacobs, and J. L. Pasquier, "The assessment and management of risks associated with exposures to short-range Auger- and beta-emitting radionuclides. State of the art and proposals for lines of research," *J. Radiol. Protection*, vol. 33, no. 1, pp. R1–R16, Mar. 2013.
[43] M. Mossalam, A. S. Dixon, and C. S. Lim, "Controlling subcellular delivery to optimize therapeutic effect," *Theory Delivery*, vol. 1, pp. 93–169, Jul. 2010.
[44] G. Landry, B. Reniers, J. P. Pignol, L. Beaulieu, and F. Verhaegen, "The difference of scoring dose to water or tissues in Monte Carlo dose calculations for low energy brachytherapy photon sources," *Med. Phys.*, vol. 38, pp. 1526–1533, Mar. 2011.
[45] K. T. Butterworth, S. J. McMahon, F. J. Currell, and K. M. Prise, "Physical basis and biological mechanisms of gold nanoparticle radiosensitization," *Nanoscale*, vol. 4, pp. 4830–4838, Aug. 2012.
[46] J. F. Hainfeld, D. N. Slatkin, T. M. Focella, and H. M. Smilowitz, "Gold nanoparticles: A new X-ray contrast agent," *Brit. J. Radiol.*, vol. 79, pp. 248–253, Mar. 2006.
[47] C. Carnovale, G. Bryant, R. Shukla, and V. Bansal, "Identifying trends in gold nanoparticle toxicity and uptake: Size, shape, capping ligand, and biological corona," *ACS Omega*, vol. 4, no. 1, pp. 242–256, Jan. 2019.
[48] W. Roa, X. Zhang, L. Guo, A. Shaw, X. Hu, Y. Xiong, S. Gulavita, S. Patel, X. Sun, J. Chen, R. Moore, and J. Z. Xing, "Gold nanoparticle sensitize radiotherapy of prostate cancer cells by regulation of the cell cycle," *Nanotechnology*, vol. 20, no. 37, Sep. 2009, Art. no. 375101.

YA-YUN HSIAO received the Diploma degree in physics and the M.S. degree in life science from National Tsing Hua University, Hsinchu, Taiwan, in 1999 and 2001, respectively, and the Ph.D. degree in physics from Purdue University, West Lafayette, IN, USA, in 2008. She is currently an Assistant Professor with the Department of Medical Imaging and Radiological Sciences, Chung Shan Medical University, Taichung, Taiwan. Her current research interests include medical dosimetry, and evaluation of the quality and effectiveness of radiation treatment and exposure.

FENG-CHUN TAI received the B.S., M.S., and Ph.D. degrees with the Department of Electrical Engineering, National Chung Hsing University, Taichung, Taiwan, in 2007, 2010, and 2018, respectively. Since 2018, he has been holding a postdoctoral position with the Advanced Electrical Control Laboratory, Department of Electrical Engineering, National Chung Hsing University. His current research interests include mobile robots, intelligent control, navigation systems, and their applications to industrial processes and machines.

CHUN-CHIEH CHAN received the B.S. degree in electrical engineering from National Formosa University, Yunlin, Taiwan, in 2005, the M.S. degree from the Department of Electrical Engineering, National Chung Cheng University, Chiayi, Taiwan, in 2007, and the Ph.D. degree from the Department of Electrical Engineering, National Chung Hsing University, Taichung, Taiwan, in 2020. His current research interests include computer vision, intelligent control, robotic motion planning, and its applications to human–robot collaboration, human-safe systems, and biomedical engineering.

CHING-CHIH TSAI (Fellow, IEEE) received the Diploma degree in electrical engineering from the National Taipei Institute of Technology, Taipei, Taiwan, in 1981, the M.S. degree in control engineering from National Chiao Tung University, Hsinchu, Taiwan, in 1986, and the Ph.D. degree in electrical engineering from Northwestern University, Evanston, IL, USA, in 1991. From 2003 to 2005, he served as the Director for the Center for Research Development and Engineering Technology, College of Engineering, National Chung Hsing University. In 2006, he served as the Director for the Center for Advanced Industry Technology and Precision, National Chung Hsing University. He is currently a Life Distinguished Professor with the Department of Electrical Engineering, National Chung Hsing University (NCHU), Taichung. He has published and coauthored more than 500 technical articles. His current research interests include image processing and recognition, embedded systems, advanced control methods, intelligent control systems, and their applications to commercial and industrial products, mobile robots, and intelligent machinery. He is a Fellow of the IET, the CACS, and the RST. From 2012 to 2016, he served two terms as the President for the Chinese Automatic Control Society (CACS), Taiwan. From 2016 to 2019, he served two-terms as the President for the Robotics Society of Taiwan (RST) and the Vice President for the International Fuzzy Systems Association (IFSA). In 2019, he has served as the President Elect for IFSA and the Vice Dean, the R&D Office, NCHU. In 2006, he served as the Chair for the Taipei Chapter of the IEEE Robotics and Automation Society. Since 2009, he has been the Chair of the Taichung Chapter of the IEEE Systems, Man and Cybernetics Society (SMCS).